sciendo

ANNALS OF WEST UNIVERSITY OF
TIMISOARA PHYSICS
Vol. LXVII, 2025

DOI: 10.2478/awutp-2025-0005

EFFECT OF PROCESS PARAMETERS ON THE PROPERTIES OF YTTRIUM OXIDE CERAMICS

Vasilica Țucureanu*[a], Oana Brîncoveanu, Cosmin Romanițan,
Iuliana Mihalache, Alina Matei*[b]

National Institute for Research and Development in Microtechnologies (IMT-Bucharest),
Erou Iancu Nicolae Street, 126A, 077190, Bucharest, Romania
**Corresponding author: e-mail: [a]vasilica.tucureanu@imt.ro; [b]alina.matei@imt.ro*

Article Info

Received: 13.08.2025
Accepted: 03.10.2025

Keywords:
Y_2O_3, Y_2O_3:Eu, hydrothermal process, ceramics

Abstract

The demand for innovative materials with multiple properties, that are economically feasible, has opened the way for materials such as polycrystalline transparent ceramics. These ceramics have the advantage of materials with high mechanical resistance, good thermal and chemical stability, optical transparency, biocompatibility, adaptable properties, transmission range from UV to IR, the possibility of doping with rare earths. In addition, they have found their utility in aerospace and military applications, the manufacturing of high-temperature IR windows or armored windows, electro-optical devices, lasers, scintillators, catalysts, fluorescent markers etc. In this paper, we studied the influence of process parameters on the hydrothermal synthesis of yttrium oxide ceramics. Practically, we used yttrium nitrate and urea in the presence of polyethylene glycol, and the colloidal precipitate was transferred to a 40 ml autoclave and maintained at 150°C for 12 h. The resulting precursor was subjected to a thermal treatment at 600°C for 3 h. The effects of the process parameters on the structure, morphology and optical properties were investigated in detail. The transition from the precursor to the crystalline phase of yttrium oxide was observed by Fourier Transform Infrared (FTIR) spectrometry and X-ray diffraction (XRD). FTIR spectroscopy confirmed the formation of M-O bonds, while XRD data demonstrated the progression of the crystalline phase. The particles' spherical form and rounded edges were seen at SEM. The optical investigations validated the utility and suitability of the proposed method for the production of yttrium oxide-based ceramics.

1. Introduction

Polycrystalline transparent ceramics (PTC) represent a class of advanced materials with applications in various fields, due to a unique combination of mechanical, thermal, chemical, and optical properties [1]. Generally, optical materials are transparent to electromagnetic waves of ultraviolet (up to 380 nm), visible (380–780 nm), and infrared (780–2000 nm) regions [2]. Technological progress in recent decades has made it possible to tailor particle

morphology, their interconnectivity, and structural orientation to direct their physicochemical and mechanical properties for applications in the military, aerospace, medical, energy, and other civilian sectors. The general steps for obtaining a polycrystalline ceramic material involve: preparation of high-purity powder, to prevent light absorption by impurities, with submicron size, with or without dopants (by sol-gel methods, coprecipitation, etc.), followed by powder pressing steps (cold or hot isostatic pressing, slip casting, hot pressing, spark plasma sintering), thermal treatment to remove residual pores and obtaining complete densification (vacuum hot pressing, spark plasma sintering), and polishing to reduce roughness [2-5]. Polycrystalline submicron alumina, aluminum oxynitride, yttrium oxide, yttrium aluminum garnet, zirconium oxide, zinc sulfide, are some examples of transparent ceramic materials reported in the literature [1, 6, 7].

Yttrium oxide or yttria (Y_2O_3) is one of the 17 essential rare earth oxides, which appears in the form of white powder. Y_2O_3 exhibits a high energy band gap (~5.7 eV), low phonon energy (380 cm^{-1}), high refractive index (~2, at 550 nm), optical transparency in the visible and infrared, high thermal conductivity and hardness, and excellent chemical and thermodynamic stability (melting point ~2430°C) [7-9]. Y_2O_3 has been used as transparent a polycrystalline ceramic in applications, such as: optical or protective windows for high-power lasers (Y_2O_3:Yb^{3+}, YAG:Nd,), medical or military guidance systems, sensors, screens in the nuclear field etc [3, 4, 10]. Moreover, Y_2O_3 is one of the most commonly used phosphor host materials, which through (co)doping (Yb^{3+}, Tm^{3+}, Pr^{3+}, Gd^{3+}, Nd^{3+}, Eu^{3+} etc.) or in combination with other oxides (e.g. with Al_2O_3 in YAG) acquires remarkable physicochemical properties, that enable the absorption of electromagnetic radiation and its conversion into vissible emission (yellow phosphor YAG:Ce, red phosphor Y_2O_3:Eu), as a result of the gradual excitation between the discrete energy levels of the rare earth ions [4, 11-14]. Considering the advantages offered by this type of oxide, the synthesis technology plays a fundamental role, therefore different methods have been investigated, including (co)precipitation, sol-gel, hydro-/solvothermal, spray pyrolysis, microplasma-assisted, solution combustion, detonation or eco-friendly approaches [7, 9, 15, 16]. However, these methods still present disadvantages deriving from a high degree of complexity, poor control over purity and morphology, high consumption of raw materials, time, energy, and negative impact on the environment.

Synthesis of transparent Y_2O_3 ceramics is an advanced process that requires rigorous control of material purity and particle morphology to avoid light absorption and scattering. Considering the advantages of hydrothermal processes (good control of particle size and

shape, high crystallinity, and purity, lower synthesis temperature, stability and reproducibility), this study aims to investigate the possibility of synthesizing Y_2O_3 particles using hydrothermal synthesis and the influence of Eu^{3+} ions for the development of fluorescent materials. Structural properties were studied using XRD, FTIR and EDX spectroscopy, while SEM was employed to assess the morphological features. The optical properties, determined by PL spectrometry, confirm the application potential of these materials.

2. Method and samples

For the synthesis of Y_2O_3 and Y_2O_3:Eu by the hydrothermal method, we used the following analytical grade starting materials, purchased from Merck: yttrium (III) nitrate hexahydrate ($Y(NO_3)_3 \cdot 6H_2O$), europium (III) nitrate pentahydrate ($Eu(NO_3)_3 \cdot 5H_2O$), urea (NH_2CONH_2) and polyethylene glycol (PEG, $H(OCH_2CH_2)_nOH$, Mw=1000). During the process, deionized water (DIW) was used for the synthesis and washing of the oxide precursor.

The structural, morphological, optical evolution, and wetting capacity of the samples were studied using the following equipment: The characterization techniques involved are (i) Rigaku SmartLab X-ray Diffraction System used to study the crystallinity and phase identification for the studied materials; (ii) Bruker Tensor 27 FTIR spectrometer for identifying the chemical bond configuration of precursor and oxide samples; (iii) FEI Nova NanoSEM 630 system having an EDAX facility provide information about morphological and compositional analysis; (iv) photoluminescence spectra were recorded on an FLS-920T spectrometer equipped with an integrating sphere.

The synthesis of submicron undoped and Eu^{3+} doped Y_2O_3 particles was performed using a hydrothermal process that involves the use of $Y(NO_3)_3 \cdot 6H_2O$ and $Eu(NO_3)_3 \cdot 5H_2O$ as a source of cations, and urea as a capping and reducing agent. Urea is a biodegradable compound that does not produce hazardous contamination byproducts [17]. Also, to reduce the tendency of agglomeration and increase hydrophilicity, we used a second compound as capping agent, biocompatible and eco-friendly compound. The process for the synthesis of Y_2O_3 follows two main steps: (a) hydrothermal synthesis, in liquid medium, of the precursor and (b) thermal treatment, in solid phase, which finalizes the morphology and crystalline structure. In the precursor production stage, the synthesis reaction is carried out inside an autoclave with an outer high-quality stainless steel jacket and an inner Teflon liner or chamber. In the first stage, the stock solutions of $Y(NO_3)_3 \cdot 6H_2O$ with a concentration of

5 mmol/l, $Eu(NO_3)_3 \cdot 5H_2O$ with a concentration of 5 mmol/l and urea with a concentration of 0.02 mol/l were prepared. The initial solution consists of PEG in a 1:1 ratio towards ADI, to which the nitrate and urea were added simultaneously. The colorless solution thus obtained was stirred for 60 min. at room temperature. An excess of urea was used, maintaining a nitrate:urea ratio of 1:4, and the dopant was added in a proportion of 8%. This reaction mixture was transferred to autoclave, leaving about 25% of its volume, and the placed in an oven heated to 150 °C for 12 h. The reaction solution was allowed to cool to room temperature before being collected and subjected to successive decantation and washing operations by: centrifugation at 9000 rpm, 10 min, removal of the supernatant and redispersion in water, to eliminate by-products or unreacted substances. The thermal treatment step involves slow drying, overnight, in a desiccator of the precursor, followed by slow treatment of the precursors up to a maximum of 600°C, with a furnace heating rate of 7°C/min and maintaining for 3 h.

3. Results and Discussions

3.1. Structural Analysis

From the structural point of view, Y_2O_3 exhibits three distinct crystallization phases, namely: cubic (cI80), monoclinic (mP30), and hexagonal (hP10). Among these, the cubic phase is the most thermodynamically stable, and has been studied for the use of Y_2O_3 in emissive applications. At room pressure, Y_2O_3 exhibits a cubic structure; however, by increasing the pressure, it can transform into either the phases (cubic → monoclinic → hexagonal or cubic → hexagonal). It was also found that plastic deformation can induce a structural transformation from the cubic to the monoclinic phase [11,18].

The purity and crystallinity of Y_2O_3 particles (doped and undoped) obtained by hydrothermal method in the absence and presence of PEG, and subsequently subjected to thermal treatment at 600°C for 3 h, were examined using the X-ray diffraction pattern shown in Figure 1.

One can observe that the diffraction peaks associated with the precursor completely disappear at the synthesis temperature up to 600°C, and the XRD data of the oxide powders confirm the formation of a material with a cubic crystalline structure. For all Y_2O_3 samples, each diffraction peak was indexed according to ICDD (International Center for Diffraction Data) cards no 100-9013 and 79-1716 [19]. The lattice parameters were calculated and presented in Table 1.

Table 1. The parameters assigned to X-Ray diffraction peaks of Y_2O_3 without PEG, Y_2O_3 with PEG, and Y_2O_3:Eu with PEG samples.

Sample				*Y_2O_3 without PEG*	*Y_2O_3 with PEG*	*Y_2O_3:Eu with PEG*
Crystal system:	Structure			Cubic	Cubic	Cubic
	Space group			206 : Ia3	206 : Ia3	206 : Ia3
Cell parameters:	Constant lattice (Å)			10.6128	10.6060	10.6278
	Atomic cell volume ($Å^3$)			1195.3358	1193.0396	1200.4114
Average crystallite size (nm)				13.2	23.1	25.6
Phase name:	*Miller indices*			*2θ (°)*	*2θ (°)*	*2θ (°)*
	h	*k*	*l*			
Yttria (Y_2O_3)	2	1	1	20.42	20.47	20.59
Yttria (Y_2O_3)	2	2	2	29.08	29.08	29.18
Yttria (Y_2O_3)	4	0	0	33.68	33.70	33,79
Yttria (Y_2O_3)	4	1	1	35.80	35.85	35.97
Yttria (Y_2O_3)	4	2	0	-	37.84	38.03
Yttria (Y_2O_3)	3	3	2	39.70	39.78	39.82
Yttria (Y_2O_3)	4	3	1	43.49	43.41	43.47
Yttria (Y_2O_3)	5	2	1	-	46.84	46.89
Yttria (Y_2O_3)	4	4	0	48.45	48.46	48.51
Yttria (Y_2O_3)	4	3	3	-	50.06	50.14
Yttria (Y_2O_3)	6	1	1	52.99	53.13	53.23
Yttria (Y_2O_3)	6	2	0	-	54.65	54.79
Yttria (Y_2O_3)	5	4	1	56.08	56.14	56.11
Yttria (Y_2O_3)	6	2	2	57.53	57.54	57.58
Yttria (Y_2O_3)	6	3	1	58.88	59.00	59.01
Yttria (Y_2O_3)	4	4	4	60.29	60.41	60.43
Yttria (Y_2O_3)	5	4	3	-	61.78	61.79
Yttria (Y_2O_3)	6	4	0	-	63.15	63.24
Yttria (Y_2O_3)	7	2	1	64.46	64.49	64.55
Yttria (Y_2O_3)	7	3	2	-	69.69	69.79
Yttria (Y_2O_3)	8	0	0	71.05	71.02	71.09
Yttria (Y_2O_3)	8	1	1	-	72.28	72.28
Yttria (Y_2O_3)	8	2	0	-	73.49	73.31
Yttria (Y_2O_3)	6	5	3	-	74.85	74.75
Yttria (Y_2O_3)	8	2	2	-	76.06	76.26
Yttria (Y_2O_3)	8	3	1	-	77.31	77.27
Yttria (Y_2O_3)	6	6	2	78.59	78.49	78.49
Yttria (Y_2O_3)	8	4	0	80.91	80.97	80.97
Yttria (Y_2O_3)	8	5	1	87.04	87.05	87.05
Yttria (Y_2O_3)	9	3	2	-	89.54	89.54
Yttria (Y_2O_3)	8	4	4	90.77	90.70	90.70

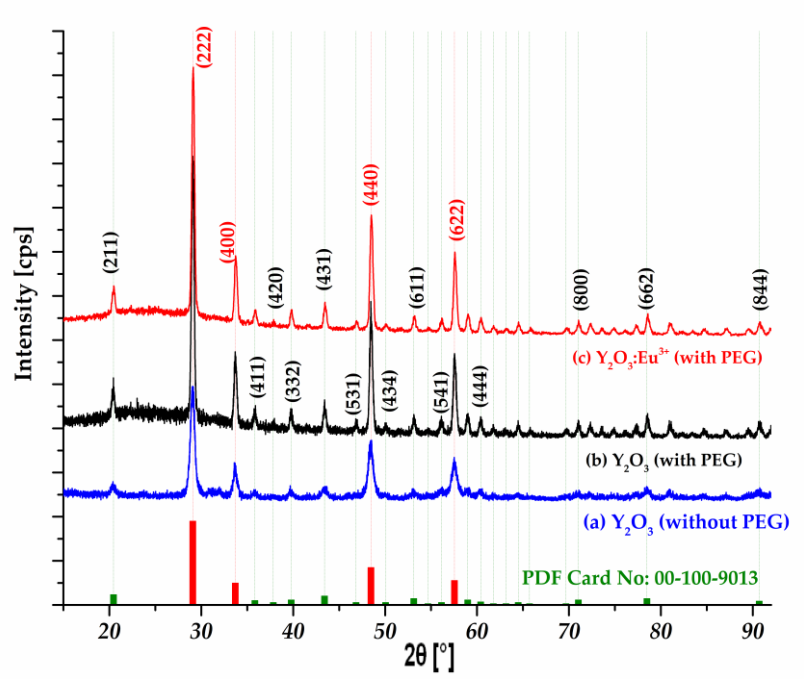

Figure 1. XRD patterns of the Y_2O_3 and $Y_2O_3:Eu^{3+}$ synthesized in the presence and absence of PEG, after thermal treatment at 600°C

The three main characteristic diffraction peaks of Y_2O_3 were found, at 2θ = 29.08°, 48.45° and 57.53°, further indexed as (222), (440) and (622) Miller planes, while the low intensity peaks were assigned to a cubic crystal structure belonging to a space group 206:Ia3. This phase corresponds to a BCC (body-centered cubic) structure, also known as bixbyite, C-type or C-Y_2O_3 structure [16, 20, 21]. In all three XRD patterns, no peaks indicating the presence of secondary phases were observed, which confirm the complete decomposition of the complex precursor and the formation of high-purity Y_2O_3. Also, for the doped sample, no additional peaks associated with a crystalline phase involving Eu^{3+} were observed, demonstrating the incorporation of Eu^{3+} ions by substitution of Y^{3+} ions, which shows that the prepared samples are single-phase, and the substitution of the Eu^{3+} ion in the Y_2O_3 structure occurred homogeneously during the reaction. The unit cell of Y_2O_3 is composed of 80 atoms (48 O and 32 Y, being considered a combination of 64 cubic sections) for which the lattice constants were found in agreement with the data from standard cards (a=b=c=10.6056 Å) or reported in the literature (10.6040 Å) [18]. For the samples obtained in the presence of PEG, the observed peaks are sharper and with higher intensity, which certifies a greater degree of crystallinity of the Y_2O_3 particles obtained in the presence of this surfactant [21]. By substituting yttrium ions and introducing the dopant into the crystal lattice in the form of trivalent Eu ions, with a larger ionic radius (r_i (Y^{3+}) = 0,9 Aº, $r_i(Eu^{3+})$ = 0.947 Aº), the lattice parameters are modified, as a consequence of the crystalline structure

deformation. The lattice strain for Y_2O_3 samples is ~ 0.08% at 600°C, around, increasing to ~ 0.17% for Y_2O_3:Eu. Using the Williamson-Hall method, a mean crystallite size of approximately 26 ± 3 nm was found for Y_2O_3:Eu. The data were consistent with those obtained using the main peak and the Scherrer equation, taking into account the spherical shape of the crystallites, for which the *k* factor is 0.93.

FTIR spectroscopy was used to evaluate the nature of interactions that occur during the synthesis processes of ceramic particles. Figure 2 shows the FTIR spectra of the main raw materials involved in the process (yttrium nitrate and polyethylene glycol), as well as the spectra of the reaction products from the hydrothermal stage (the oxide precursor), and after the thermal treatment (yttrium oxides). The FTIR spectrum of yttrium nitrate hexahydrate is mainly defined by the bands associated with the nitrate ion, as well as adsorbed water molecules. In the ranges 4000-3000 and 1700-1600 cm^{-1}, bands are observed that confirm the presence of water of crystallization [7]. The other bands in the 1600-1000 cm^{-1} range are due to stretching and bending vibrations of the NO_3^- group, and the absorption bands centered at 812, 749, 723, and 648 cm^{-1} indicate the interaction between the yttrium cation and the nitrogen anion [22-24].

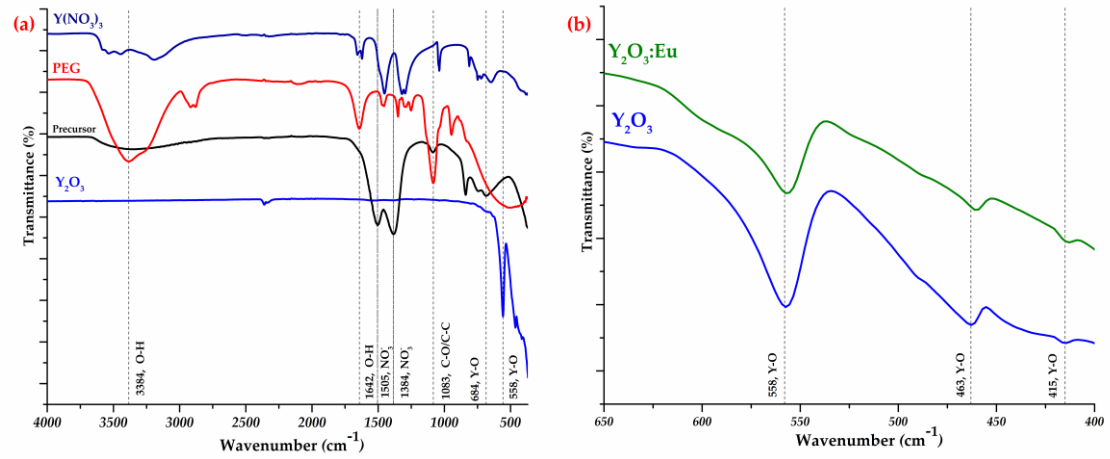

Figure 2. FTIR spectra for the raw materials and reaction products: yttrium nitrate, PEG, oxide precursor, Y_2O_3, and Y_2O_3:Eu (a), and detail highlighting the bands associated with Y-O bonds, on the 650-370 cm^{-1} range (b)

The PEG spectrum shows characteristic bands that can be assigned to terminal OH groups (3384, 1642 cm^{-1}), ether chains, C-O-C (1300-1000 cm^{-1}) and methylene chains, $-CH_2-$ (2916, 2881, 1456, 1350, 947 and 842 cm^{-1}) [25, 26]. The FTIR spectrum of the precursor obtained through the hydrothermal process suggests the formation of a complex precursor of the hydroxynitrate type, $Y(OH)_{3-x}(NO_3)_x$. The band centered at 3361 cm^{-1} can be attributed to O-H stretching vibrations from both the hydroxynitrate and PEG. The high

intensity bands centered at 1505 and 1384 cm^{-1} are associated with the symmetric and asymmetric stretching vibration of the nitrate ion in the complex, respectively [27]. The presence of the organic component in the precursor is confirmed by the appearance of the low intensity band centered at 1086 cm^{-1}, which can be attributed to the vibration mode of the ether bonds in the polyethylene glycol chain [28, 29]. The band centered at 684 cm^{-1} can be assigned to the vibration mode of the Y-O(H) bonds. During the thermal treatment, the dehydroxylation of $Y(OH)_{3-x}(NO_3)_x$ begins, and at 600°C the complete decomposition of the precursor is observed, the removal of nitrates, hydroxides, and the organic component, from the structure, which indicate the use of a sufficient temperature for the total decomposition and complete removal of of the secondary reaction products, and the formation of a high-purity yttrium oxide. At lower wavenumbers than 600 cm^{-1} (558, 463 and 415 cm^{-1}) the spectrum of oxide particles is characterized by absorption bands corresponding to the stretching vibrations of Y-O and Y-O-Y bonds in cubic Y_2O_3 [9, 30-32]. Doping with Eu^{3+} ions is indirectly confirmed, by a slight shift of these absorption bands to lower wavenumbers (554, 459 and 412 cm^{-1}). The absence of new bands indicates that Eu^{3+} is inserted into the cubic lattice, without forming secondary phases of Eu_2O_3 without altering the Y_2O_3 structure. The shift of the absorption bands may result from the difference in ionic radii between the two cations. The Eu^{3+} ion has a slightly radius larger than Y^{3+} in sixfold coordination (r_i (Y^{3+}) = 0,9 Å, $r_i(Eu^{3+})$ = 0.947 Å) leading to local lattice expansion and a weakening of the Y-O bonds vibrations. These results confirm the observations from the XRD diffractogram.

To evaluate the chemical composition at the atomic level, Figure 3 presents the EDX spectra for Y_2O_3 and Y_2O_3:Eu samples, obtained in the presence of PEG and subjected to a thermal treatment at 600°C for 3h. From the point of view of qualitative analysis, peaks were identified in the two oxide spectra that can be attributed to atoms of oxygen (O(K) at 0.52 keV) and yttrium (Y(L) at 1.92 keV) [24]. In the spectrum of the doped oxide, low intensity drops corresponding to dopant atoms (Eu(L) at 5.84 keV and Eu(M) at 1.14 keV) were identified. Quantitative analysis shows that the weight of the constituent elements is in accordance with the structural formula of the oxides and close to the calculated stoichiometry, estimating the obtaining of a final product with a structural formula close to the theoretical ones $Y_{1.98}O_{3.02}$ and $Y_{1.91}Eu_{0.08}O_{3.01}$, respectively, and an Eu:Y atomic ratio of 0.0421. Except the peak due to the substrate (Si(K) at 1.739 keV), no other impurities could be identified.

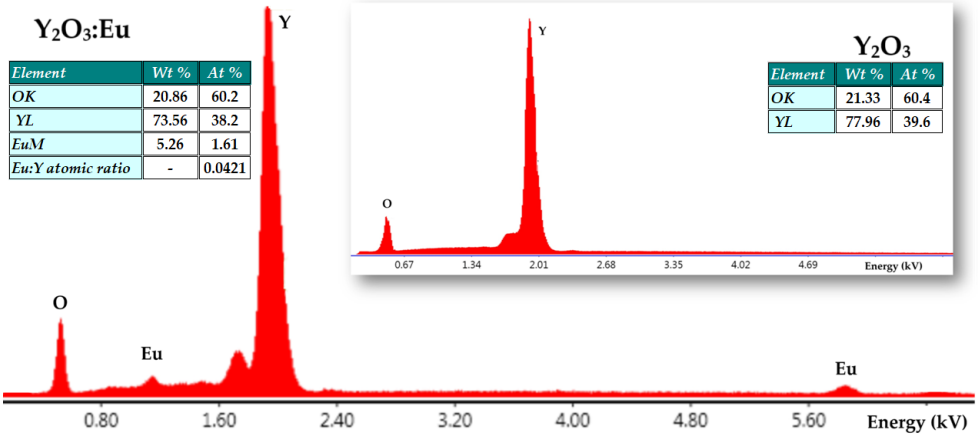

Figure 3. EDX spectra for Y_2O_3 and Y_2O_3:Eu, obtained in the presence of PEG, after the thermal treatment at 600°C

3.2. Morphological Analysis

The agglomeration of the powder influence densification and grain growth rates, which negatively influences the formation of final ceramic products [3]. Scanning electron microscopy (SEM) was used to study the shape, size, defects and the agglomeration tendency of oxide particles. Figure 4 illustrates the morphology of the yttrium oxide samples obtained in the presence of PEG, and after a thermal treatment at 600°C. The particle morphology appears to be constant, suggesting a controlled synthesis process. The approximate size distribution of the oxide particles was determined from the SEM images by measuring about 200 particles, using the "Image J" software [33]. Subsequently, the data were compiled into the histogram shown, as in Figure 4b, which was fitted with a Gaussian function to best represent the distribution.

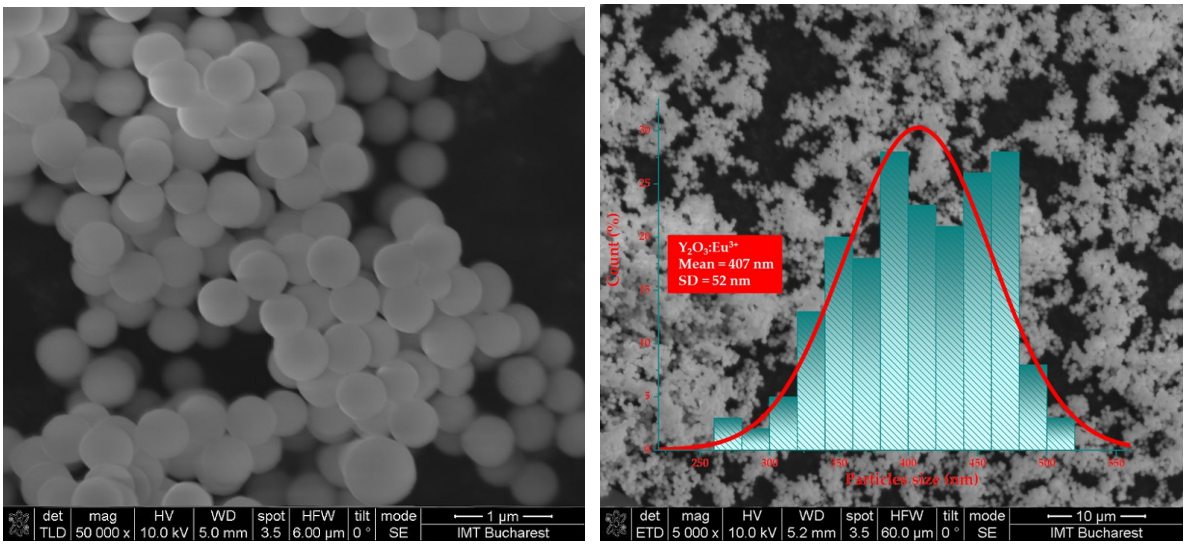

(a) (b)

Figure 4. SEM micrograph of a representative sample of Y_2O_3, obtained by the hydrothermal method in the presence of PEG, and after a thermal treatment at 600°C (a); and
Histogram with normal distribution of the size for Y_2O_3:Eu (b)

From image analysis, one can observe spherical particles with submicron dimensions, with well-defined boundaries, without surface defects. No agglomeration tendency was observed, indicating high crystallinity. Their diameter ranges from 250 to 510 nm, with an average diameter of approximately 410 nm. The dopant does not influence the morphology of the particles.

3. 3. Optical Analysis

Demonstration of the utility and feasibility of using yttrium-based ceramic materials can be achieved through fluorescence spectrometry. Doping Y_2O_3 with different rare-earth ions can produce materials with emissive properties in different spectral ranges, which have found application from the biomedical field to optoelectronics. In the following, the emissive properties of the $Y_2O_3:Eu^{3+}$ ceramic product obtained by excitation with a radiation at 465 nm were studied and illustrated in figure 5.

The emission spectra for the phosphors samples obtained, in the presence and absence of PEG, showed a series of emission maxima between 550 and 700 nm, which can be associated with the $^5D_0 \rightarrow {}^7F_J$ (J=0-4) electric dipole transition of the Eu^{3+} ions in the Y_2O_3 host lattice. The spectra of the samples are dominated by the $^5D_0 \rightarrow {}^7F_2$ transitions which allow emission in the red (~610 and 630 nm). Additionally, lower intensity emission bands, centered around 580 nm, can be attributed with the $^5D_0 \rightarrow {}^7F_0$ transition, those at 587, 583 and 599 nm to the $^5D_0 \rightarrow {}^7F_1$ transition, at 650 and 662 nm to the $^5D_0 \rightarrow {}^7F_3$ transition, and the bands at 687, 693 and 599 nm to the $^5D_0 \rightarrow {}^7F_4$ transition [9, 21, 34]. The increase in the degree of crystallinity for the samples obtained in the presence of PEG is observed from the structural analysis, and is confirmed by the increase in the emission intensity of phosphor. These results indicate that transparent $Y_2O_3:Eu^{3+}$ ceramic is a promising candidate for use as a color converter.

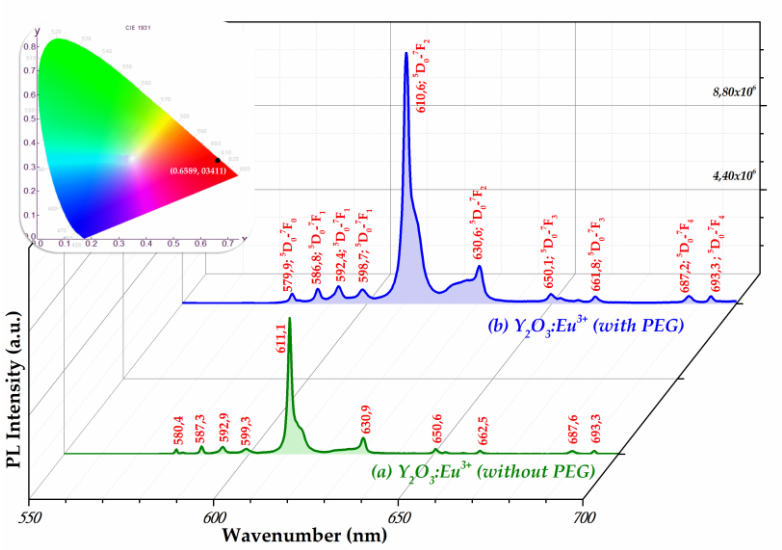

Figure 5. PL excitation spectra of $Y_2O_3:Eu^{3+}$ ceramic and the CIE chromaticity diagram

The CIE chromaticity diagram (introduced by the Commission International de L'Éclairage in 1931) for $Y_2O_3:Eu^{3+}$ ceramic under 465 nm excitation provides an intuitive view of the red emission colors. According to McCamy's formula ($n = (x-0.3320)/(0.1858-y)$; $CCT = 437 \cdot n3 + 3601 \cdot n2 + 6861 \cdot n + 5517$), the Correlated Color Temperature (CCT) can be calculated from the CIE coordinates with an error of ±2 Kelvin degree [15]. For the coordinates (0.6589; 0.3411), the CCT ≈ 2955 Kelvin was calculated, which corresponds to "warm" light emission.

4. Conclusions

We have obtained yttrium oxide by the hydrothermal method, which is a synthetic ceramic material. By doping with Eu^{3+} ions, we developed a transparent ceramic material with fluorescent properties. This method allowed obtaining the homogeneous particles with controlled submicron sizes and high purity, essential conditions for the final transparency of the ceramic and, last but not least, a decrease in the sintering temperature due to the high reactivity of the powder. The structural studies carried out by XRD, FTIR and EDX spectroscopy demonstrated the crystallinity and purity of the material, as well as the absence of secondary phases or other types of impurities associated with the synthesis process. The presence of the dopant was evidenced by EDX analysis, but also indirectly by modifying the lattice in the parameters as a result of the substitution of Y^{3+} ions with Eu^{3+} ions. The importance of using PEG in the process was highlighted by an increase in the degree of crystallinity, which translated into an enhancement in emission intensity. Optical studies performed on $Y_2O_3:Eu^{3+}$ demonstrated the potential for excitation at 465 nm and maximum

emission in the red region, around 610 nm. The chromaticity coordinates allowed us to calculate the color temperature indicating the obtaining of a device with warm light emissions. The obtained materials can be used subsequently in the production of transparent polycrystalline ceramics, intended for the development of screens or as fluorescent markers.

Acknowledgements

This work was supported by a grant of the Ministry of Research, Innovation and Digitization, CNCS-UEFISCDI, project number PN-IV-P2-2.1-TE-2023-0417 (BioYDetect, Contract no. 30TE/2025), within PNCDI IV.

References

[1] R. Johnson, P. Biswas, P. Ramavath, R. Kumar, G. Padmanabham, Trans. Indian Ceram. Soc 71(2) (2012) 73–85

[2] I. B. Oparina, A. G. Kolmakov, Refract Ind Ceram 62(2) (2021) 196-201

[3] Q. Zhu, P. F. Yang, Z. Y. Wang, P. C. Hu, J. Eur. Ceram. Soc, 40 (6) (2020) 2426-2431

[4] S. Balabanov, D. Permin, T. Evstropov, P. Andreev, L. Basyrova, P. Camy, M. Baranov, X. Mateos, P. Loiko, Opt. Mater. 119(111349) (2021) 1-17

[5] D. Hu, X. Liu, Z. Liu, X. Li, F. Tian, D. Zhu, Z. Yang, L. Wu, J. Li, Magnetochemistry 7(6) (2021) 1-13

[6] O. J. Akinribide, G. N. Mekgwe, S. O. Akinwamide, F. Gamaoun, C. Abeykoon, O. T. Johnson, P. A. Olubambi, J. Mater. Res. Technol. 21, 7 (2022) 12-738

[7] S. Kumar, H. Tripathi, S. Bhardwaj, D. Garbiec, A. Gupta, U. Batra, J. D. Sharma, J. Mol. Struct., 1302 (2024) 137463

[8] K. B. Narayanan, H. H. Park, Adv. Colloid Interface Sci 201–202 (2013) 30–42

[9] X. Li, X. Liu, J. Qian, T. Zhang, B. Sun, Y. Han, Ceram. Int. 50 (2024) 27995–28003

[10] T.M. Abdalkreem, H.C. Swart, R.E. Kroon, Nano-Struct. & Nano-Obj. 35 (2023) 101026

[11] S. G. Nath, E.I. Anila, Ceram. Int. 49 (2023) 13200–13207

[12] E. Hasabeldaim, H.C. Swart, R.E. Kroon, Phys. B 671 (2023) 415417

[13] H. M. Oh, H.N. Kim, Y.J. Park, J.W. Ko, H. K. Lee, Opt. Mat. 121 (2021) 111562

[14] W. Liu,Y. Wangn, M. Zhang,Y. Zheng, Mat. Lett. 96 (2013) 42–44

[15] J.V. Kavya, G. Jyothi, Veena Lalan, K.G. Gopchandran, Chem. Phys. Impact 8 (2024) 100576

[16] A. Matei, V. Țucureanu, B. C. Ţîncua, M. Avram, C. Romanițan, M. C. Popescu, J. Optoelectron. Adv. Mater. 21(7-8) (2019) 541 - 546

[17] J. Z.Marinho, F. C. Romeiro, S. C. S. Lemos, F. V.Motta, C. S. Riccardi, M. S. Li, E. Longo, R. C. Lima, Journal of Nanomater 2012 (2012) 427172

[18] V. Krupa, A. Dasgupta, C. Ghosh, S. K. Sinha, J. Alloys Compd. 900 (2022) 163550

[19] V. Țucureanu, C. Romanițan, I. Mihalache, A. Matei, Mater. Sci. Eng. B 311 (2025) 117808

[20] R.J. Gaboriaud, F. Paumier, B. Lacroix, Thin Solid Films 601 (2016) 84–88

[21] G. Zhou, Y. Li, Y. Ma, Z. Liu, L. Cao, D. Wang, S. Liu, W. Xu, W. Wang, J Nanopart Res 18 (2016) 135

[22] J. L. Bishop, S. J. King, M. D. Lane, A. J. Brown, B. Lafuente, T. Hiroi, R. Roberts,
G. A. Swayze, J.-F. Lin, M. S. Roman, Earth Space Sci 8 (2021) e2021EA001844

[23] M.Y. Mihaylov, V.R. Zdravkova, E.Z. Ivanova, H.A. Aleksandrov, P.St. Petkov, G.N. Vayssilov, K.I. Hadjiivanov, J. Catal. 394 (2021) 245–258

[24] M.Y. Mihaylov, V.R. Zdravkova, E.Z. Ivanova, H.A. Aleksandrov, P.St. Petkov, G.N. Vayssilov, K.I. Hadjiivanov, J. Catal. 394 (2021) 245-258.

[25] N. S. Vrandecic, M. Erceg, M. Jakic, I. Klaric, Thermochim. Acta 498 (2010) 71–80

[26] M. Sahu, V. R. M. Reddy, B. Kim, B. Patro, C. Park, W. K. Kim, P. Sharma, Materials 15 (2022) 1708

[27] V. Ţucureanu, C. Romaniţana, I. A. Tudor, C. Ţucureanu, M. A. Popescu, A. Matei, Ceram. Int. 46 (2020) 23802–23812

[28] V. Ţucureanu, C.A. Obreja, G. Crăciun, C. Romaniţan, C. M. Mihăilescu, D. Stan, A. Matei, Ceram. Int. 48 (2022) 27201–27212

[29] J. Lenga, J.Tang, W. Xie, J. Lia, L. Chen, Mat. Res. Bull. 100 (2018) 171–177

[30] X. Li, X. Liu, J. Qian, T. Zhang, B. Sun, Y. Han, Ceram. Int. 50 (2024) 27995-28003.

[31] V. Tucureanu, A. Matei, A.M. Avram, Opto−Electron. Rev. 23(4), (2015) 239–251

[32] S. Kumar, H. Tripathi, S. Bhardwaj, D. Garbiec, A. Gupta, U. Batra, J.D. Sharma, J. Mol Struct. 1302 (2024) 137463.

[33] Schneider, C. A., Rasband, W. S. & Eliceiri, K. W. (2012). Nat. Methods, 9, 671–675.

[34] M. Zhang, X. Li, Z. Wang, Q. Hu, H. Guo, Trans. Nonferrous Met. Soc. China, 20(1) (2010) 115-118